

## FRONT MATTER

### Atomic Scale Structural Identification and Evolution of Co-W-C Ternary SWCNT Catalytic Nanoparticles: HR-STEM imaging on SiO<sub>2</sub>

Hua An,<sup>1†</sup> Akihito Kumamoto,<sup>2†</sup> Rong Xiang,<sup>1\*†</sup> Taiki Inoue,<sup>1</sup> Keigo Otsuka,<sup>1</sup> Shohei Chiashi,<sup>1</sup> Christophe Bichara,<sup>3</sup> Annick Loiseau,<sup>4</sup> Yan Li,<sup>1,5</sup> Yuichi Ikuhara<sup>2</sup>, Shigeo Maruyama<sup>1,6\*</sup>

<sup>1</sup> Department of Mechanical Engineering, The University of Tokyo, Tokyo 113-8656, Japan

<sup>2</sup> Institute of Engineering Innovation, The University of Tokyo, Tokyo 113-8656, Japan

<sup>3</sup> CINAM, CNRS and Aix Marseille Université, Campus de Luminy, Case 913, 13288 Marseille Cedex 9, France

<sup>4</sup> Laboratoire d'étude des microstructures, CNRS-ONERA, 92322 Châtillon, France

<sup>5</sup> College of Chemistry and Molecular Engineering, Peking University, Beijing 100871, China

<sup>6</sup> Energy NanoEngineering Laboratory, National Institute of Advanced Industrial Science and Technology (AIST), Tsukuba 305-8564, Japan

†These authors contributed equally to this work.

\*Corresponding author. Email: xiangrong@photon.t.u-tokyo.ac.jp (R.X.); maruyama@photon.t.u-tokyo.ac.jp (S.M.)

## Abstract

Chirality control has been the greatest challenge in chemical vapor deposition (CVD) synthesis of single-walled carbon nanotubes (SWCNT). This challenge is largely caused by the difficulties in characterizing the nano-sized catalyst particles and thereby insufficient understanding of their behaviors. Recently W-based catalyst has provided a promising route to synthesize SWCNTs with specific chirality, but the mechanism of the growth selectivity is still vaguely understood and under intensive discussion. Here we propose a strategy to identify the atomic structure, as well as the structure evolution of Co-W-C ternary catalyst. The key is to use a thin SiO<sub>2</sub> film as the catalyst support and observation window. As the catalyst can be uniformly prepared on this high-temperature stable film and directly used for SWCNT synthesis, this method possesses superior advantages over conventional methods: being able to obtain original, statistical, and dynamic understanding on the catalyst. With this technique, we illustrate that Co-W-C ternary catalyst form junctions of metallic W and  $\eta$  carbide Co<sub>6</sub>W<sub>6</sub>C after reduction. But as the CVD starts, the catalyst undergoes a W loss, which finally results in a precipitation of pure hexagonal close packed (hcp) phase metallic Co. This precipitated Co phase is fully coherent to the parent crystal, having a strict crystal orientation to Co<sub>6</sub>W<sub>6</sub>C. As a method, the current TEM imaging directly on SiO<sub>2</sub> serves as a powerful and versatile tool to investigate nanocrystals and high temperature reactions; for synthesis of SWCNTs, this work successfully visualizes the structure and evolution of catalyst, and illuminates the possible nucleation sites of chirality specific growth.

## MAIN TEXT

**The manuscript should be a maximum of 15,000 words.**

### Introduction

Single-walled carbon nanotube (SWCNT) has received a great attention since its discovery in 1993.<sup>(1, 2)</sup> This focused attention is largely driven by its one-dimensional structure, and the resulting unique physical properties.<sup>(3)</sup> One of the most interesting properties is the chirality-dependent electronic conduction, which was pioneered by M. Dresselhaus even before the observation of SWCNTs <sup>(4, 5)</sup> and intensively investigated in the past decades. In brief, depending on how a graphene sheet is rolled, each SWCNT can be described as a pair of index  $(n, m)$ , which uniquely determines the optical band structure of the tube. This correlation of chirality-property opens up a lot of interesting research for the community but at the same time brings great challenges to the controlled synthesis of SWCNT.<sup>(6-8)</sup> Chirality-pure samples are needed for the large-scale application of SWCNTs in, e.g. transistors.<sup>(9-11)</sup>

Recently, encouraging progresses have been achieved in chirality-controlled synthesis of SWCNTs using W-based solid catalysts. In 2014, F. Yang et al. proposed a  $\text{Co}_7\text{W}_6$  solid-state catalyst and achieved a chirality selective growth of  $(12, 6)$  up to 92%.<sup>(12)</sup> Later, we confirmed that a different Co-W-C ternary catalyst can be prepared by a simple method and maintain the selectivity at milder CVD conditions.<sup>(13)</sup> More recently, S. Zhang et al introduced WC and  $\text{Mo}_2\text{C}$  catalyst, and obtained horizontally aligned  $(2m, m)$  SWCNTs.<sup>(14)</sup> Though growth selectivity is clearly demonstrated after these work, the underlying mechanism is still vaguely understood and under intensive discussions.<sup>(15-18)</sup>

In all these cases, catalyst is proven to be determinative for the successful chirality-specific growth.<sup>(19)</sup> Identifying the structure and understanding the behavior of the catalyst therefore become indispensable. However, it has been extremely difficult to study the behavior of these nano-sized catalytic particles, especially, in its original morphology. Among the available characterization techniques, transmission electronic microscope is the most straightforward and powerful, but conventional transmission electron microscope (TEM) observation methods suffer from some inevitable drawbacks. For example, the information obtained could be different from the original due to compromises in the sample preparation. Even samples could be kept in their original forms, the information obtained in most cases are very local. In this context, TEM investigation on the catalyst structure in a reliable and atomic resolvable way becomes unprecedentedly important for the further control over the process.

Ideally, a reliable TEM investigation on SWCNT catalyst should meet three criteria: original (no alteration/compromise due to sample preparation), statistical (catalyst should be uniformly dispersed and the same information can be obtained everywhere), dynamic (any catalyst change before and after CVD, or the intermediate stages, can be identified). Here we present a new strategy that can meet all these three criteria. The key is to use a MEMS fabricated Si/SiO<sub>2</sub> grid, which allows us to perform catalyst preparation, SWCNT growth and atomic resolution TEM identification on the same single chip. Our  $\text{Co}_6\text{W}_6\text{C}$  catalyst is used here as an example. Its atomic structure and dynamic change are systematically studied. Two significances of this work are: 1) as a technique, the proposed TEM imaging directly on SiO<sub>2</sub> serves as a universal platform for studying many high temperature catalyst behaviors and nanomaterial synthesis; 2) for the chirality-selective growth, this study conclusively reveal the structure as junctions of metallic W and  $\text{Co}_6\text{W}_6\text{C}$ , and dynamic evolution process from  $\text{Co}_6\text{W}_6\text{C}$  to metallic Co is elucidated.

## Results

### Large area structure identification from electron diffraction

Figure 1 describes the TEM strategy proposed in this study, and the schematic structure of the chip is shown as Figure 1A and 1B. Different from conventional Cu or Mo TEM grids, our chip has two different characteristics. First, it is fully made of Si/SiO<sub>2</sub> and thermally stable up to 1000°C. Second, it is fabricated by MEMS techniques starting from a silicon wafer. These two characteristics guarantee one to perform catalyst preparation and SWCNT growth in the exact same way as a conventional substrate. Therefore, the concept is to use this Si/SiO<sub>2</sub> TEM chip to perform a transfer-free and uncompromised characterization on catalyst in their real morphologies: the same catalyst and supporting substrate as conventional CVD.

A thin suspended SiO<sub>2</sub> film serves as the observation window (Figure 1B) in our structure. The first technical challenge for this window is that SiO<sub>2</sub> is an electron insulator. Indeed, TEM imaging through this SiO<sub>2</sub> become unstable at a conventionally high electron dose due to electron accumulation (usually recognized as charge-up effect). We performed an estimate of the charge density on this SiO<sub>2</sub> window, which is shown as Figure 1C (calculation details shown in Figure S2). Briefly, the results suggest that at the same beam condition, the accumulated charge density at the edge and particularly the corner of this SiO<sub>2</sub> film is less than 10% of the value when the beam is placed at the center. Therefore, we perform most of the current study using the corner of the window. In experiment, decently high currents can be applied without bringing significant charge-up during the TEM and Scanning TEM (STEM) observations.

The catalyst studied in this work is a Co-W-C ternary system, which is able to produce (12, 6) dominant SWCNTs at a relatively milder condition. The unintentional incorporation of C to the catalyst during reduction resulted in the formation of this carbon-containing ternary catalyst, as has been discussed in our previous report (13). The chirality distribution of the produced SWCNTs is plotted in Fig. 1D. This chirality analysis is performed on a conventional Si/SiO<sub>2</sub> substrate, but a comparison of SWCNTs on the TEM chip with the conventional cases on standard Si/SiO<sub>2</sub> substrates is shown in Fig. S1, where the scanning electron microscope (SEM) images and Raman spectroscopy suggest that SWCNTs are similar. The dominant peak in Raman spectra comes from (12, 6) SWCNT, while some other peaks also appears at relatively much lower intensity. The enrichment of (12, 6) SWCNT is estimated to be 50-70%. More details on the characterization on these SWCNTs can be found in our previous report. (13) Figure 1E is a typical selected area electron diffraction (SAED) pattern of our Co-W-C catalyst prepared by sputtering. The selective area aperture used is about several μm in diameter, meaning the SAED pattern contains information from over 10,000 particles. This is the first strength for the current technique: very statistical data are obtained. The intensity profile is plotted in Fig. 1F. After comparing it with the standard pdf card (PDF#04-0806, PDF#23-0939 Fig. 1G and H), we conclude our catalyst contains two main phases: a body center cubic (bcc) metallic W phase and η carbide Co<sub>6</sub>W<sub>6</sub>C phase. This large area statistical information is hardly possible if the catalyst is not uniformly and flatly dispersed. On our grid, same results are obtained everywhere on the SiO<sub>2</sub> window. However, one should also note SAED patterns only reveal crystal phases; the amorphous compound or poorly crystallized particles, if existing, are less pronounced since they have weak diffractions. Furthermore, there is no information how such two crystals distribute on the surface. They may stay separately or form joint particles with crystal interfaces. In order to distinguish these, higher resolution STEM is employed here to directly image the crystal phases, their interfaces, and to distinguish whether or not any less-crystallized phases exist, all of which we could not answer by conventional TEM in our previous study. (13)

## Single particle structure identification from direct STEM imaging

Figure 2 presents the energy-dispersive X-ray spectroscopy (EDS) and direct STEM imaging at single particle level. Together with the SAED patterns in the previous section, the geometry and structure of catalyst can be fully illustrated. These images are taken at room temperature but similar phases are confirmed by SAED when sample is heated to higher temperatures in TEM. The EDS mappings shown in Fig. 2A-C present the elemental distribution of Co and W on the suspended SiO<sub>2</sub> film. Two types of particles can be clearly identified from this map. The type I particles are yellow, which suggests they are pure W. The type II particles are junctions of a yellow segment (pure W) and a pinkish section. This pinkish segment are mixtures of Co and W as compared in Fig. 2 B and C. In this section, we used a new atomic counting EDS technique, which gives the quantitative ratio between atoms. This analysis suggests that the overall atomic ratio is 71:29, meaning W is excessive for forming Co<sub>6</sub>W<sub>6</sub>C. This excess of W makes Co reacted with W entirely after reduction, and explains why no pure pink phase (pure Co) is observed. We believe absence of pure Co is critical for the successful growth of selective chirality, because pure Co is known to be very efficient for the growth SWCNTs with various chiralities.

More detailed structure of the junctions can be revealed by direct STEM imaging. The bottom part in Figure 2E suggest this is a metallic bcc W phase viewing from [111] direction, which corresponds to the purely yellow phase in the EDS mapping. The top part, however, is a more mixture of Co and W with a more complicated crystal structure. We tilted the sample in order to get a zone axis of this crystal domain, and the High-angle annular dark field (HAADF) and annular bright field (ABF) images are shown in Figure 2F and G. According to the SAED patterns in Figure 1, it is very likely to be Co<sub>6</sub>W<sub>6</sub>C phase. Co<sub>6</sub>W<sub>6</sub>C, known as  $\eta$  carbide, has a quite complicated cubic structure which consists of eight regular octahedra of tungsten atoms centered in a diamond cubic lattice and eight regular tetrahedra of Co atoms centered in the second diamond cubic lattice.<sup>(20)</sup> The unit cell is as long as 1 nm in each direction. To solidify the identification from SAED patterns, we simulated the STEM images of Co<sub>6</sub>W<sub>6</sub>C at different crystal directions. The comparison between experimental and simulated images in Figure 2H gives an undoubtable matching and confirms that the crystal is the [310] zone axis of Co<sub>6</sub>W<sub>6</sub>C. The particles studied here are typically 4-10 nm. Though it may be generally speculated that smaller diameter particles (e.g. ~1 nm) are more active and responsible for SWCNT growth, very small particles can be hardly found in the current catalyst. The data shown here are fairly representative; similar images can be obtained everywhere on the SiO<sub>2</sub> window, as the particles are uniformly dispersed over the surface.

A further analysis suggests that there is no clear crystal orientation relationship between Co<sub>6</sub>W<sub>6</sub>C and W after checking more particles. We emphasize this point because a different case is observed in the later part of this study (to be shown later). This absence of clear crystal orientation relationship is understandable because these two phases both have very high melting temperatures, and were possibly formed independently during the reduction process before aggregating into a junction. Nonetheless, we believe the geometry and structure of our catalyst is conclusive after this STEM imaging. The catalyst contain no noticeable amorphous phase but only two type of particles: 1) bcc metallic W and 2) junctions of W-Co<sub>6</sub>W<sub>6</sub>C. Some previous attempts use SiO<sub>2</sub> spheres, edge of carbon TEM grid as catalyst support or conventional slicing technique to visualize the catalyst.<sup>(21, 22)</sup> However, the current study convinces that it is possible to obtain atomic resolution analysis on a flat and continuous thin SiO<sub>2</sub> film, even for a very

complicated ternary structured catalyst. This high resolution serves as the second strength of our approach. This is also the first direct imaging of  $\eta$ - $\text{Co}_6\text{W}_6\text{C}$  structure.

### Dynamic Evolution of Co-W-C structure with atomic resolution

The thin  $\text{SiO}_2$  film is thermally stable at a high temperatures up to  $1000^\circ\text{C}$ , and therefore CVD can be performed on our TEM chip. The compatibility to CVD, which serves as the third strength of this technique, opens up new possibility for studies that were previously impossible. Evolution of catalyst (e.g. size change aggregation, phase change) during the reaction can be resolved. Figure 3 presents EDS mapping and the typical spectra of reduced, 1 min CVD reacted and 3 min CVD reacted Co-W-C catalyst. We found the Co-W-C catalyst particles encounter a change in morphology after the exposure to carbon source. This loss of W is unexpected as catalyst like WC was found to be very stable,<sup>(23)</sup> but it becomes possible when oxygen in ethanol interact with W via oxide or hydroxide.<sup>(13)</sup> From the EDS analysis in Figure 3B, one can see a significant decrease in relative intensity of W even after 1 min CVD. As previously noted, the current EDS can quantitatively analyze the atoms in this area, and therefore the decrease of W signal suggests that W gradually disappears during the CVD. SAED patterns of the catalyst after different CVD durations reveal the same trend (Figure S3). The relative W:Co atomic ratio decreases from 71:29 (original) to 41:59 (3 min growth).

Typical atomic structure of the 1 min and 3 min CVD reacted catalyst are shown in Figure 4. In both samples,  $\text{Co}_6\text{W}_6\text{C}$  phase persists, as can be confirmed by the experimental and simulated STEM images. However, the W phase shows a clear difference. In the former case, pure W segment (the bottom of the image) becomes a W enriched W-Co mixture according to EDS quantitative analysis. This W dominant part still exists but the size becomes much smaller than the original shapes (0 min). In the latter case, after a 3 min CVD, W enriched phases are hardly observable and typical particles (Fig. 4 D, E) contain only a single  $\text{Co}_6\text{W}_6\text{C}$  phase. This is probably because loss of W starts from this pure W phase, and  $\text{Co}_6\text{W}_6\text{C}$  structure is relatively more stable than pure W in our growth environment.

In the 3 min CVD reacted catalyst, precipitation of Co phases is observed. Figure 5 A-E show a representative particle having a junction structure. This particle is imaged from the  $[111]$  zone axis of  $\text{Co}_6\text{W}_6\text{C}$  crystal, and experimental results match perfectly with the image simulated from atomic model, as shown in Fig. 5F. However, different from the junctions in as-reduced catalyst, the current junction contains a  $\text{Co}_6\text{W}_6\text{C}$  phase and a pure Co (pink) phase. It is probably formed when the amount of W further decreases as CVD proceeds, and Co finally becomes oversaturated in a Co-W particle. The atom-resolved STEM images clearly show that the pure Co phase has a hexagonal close packed (hcp) structure, and more significantly the precipitation of Co is fully coherent to the parent  $\text{Co}_6\text{W}_6\text{C}$  structure. A coherent precipitation means that two crystals have strict crystallographic relationship, which, in the current case, can be described as  $[1\bar{1}20]$  hcp-Co //  $[111]$   $\text{Co}_6\text{W}_6\text{C}$  and  $[0001]$  hcp-Co //  $[1\bar{1}0]$   $\text{Co}_6\text{W}_6\text{C}$ , while the interface inclined from the planes of  $(0001)$  hcp-Co and  $(1\bar{1}0)$   $\text{Co}_6\text{W}_6\text{C}$ . Figure S5 are images of another particle in the same sample. The trend is similar to the previous particle but concentration of W is even lower. The precipitation of hcp Co is in contrast to many previous reports,<sup>(24-26)</sup> where SWCNTs nucleate from cobalt carbide and face-centered cubic (fcc) Co. This difference is reasonable because a parent crystal exists in the current case and acts as a template for the precipitation of Co. From both SAED and direct imaging, no noticeable pure cobalt carbide is evidenced in our catalyst. To this end, we have obtained a clear picture of the evolution happened on the Co-W catalyst during the entire CVD process.

We summarize overall process observed so far, with a ternary Co-W-C phase diagram shown in Figure 5G as a reference.<sup>(27)</sup> Though a bulk phase diagram does not explain the particle behavior or crystal interface at nanoscale, it helps to roughly understand the phase change and candidate structure. The reduced catalyst started from position in the diagram identified with red asterisk. After reduction, W is excessive so the most particles segregate into two stable compounds with fixed composition (note: not an alloy in our Co-W-C case). At this stage the Co-W-C underwent long reduction and therefore reached a thermodynamically stable two phases. However, upon the introduction of carbon source, W concentration on the surface quickly decreases, and composition moves to the left part of the diagram. In this part, the thermodynamically stable phases are  $\text{Co}_6\text{W}_6\text{C}$  and pure Co. The details of each particle and the relationship of the crystal phase can be obtained by our STEM images of each particle, which shows the precipitated Co is fully coherent to  $\text{Co}_6\text{W}_6\text{C}$ . Overall, the conclusion for our Co-W-C catalyst is that metallic W is unstable in CVD but  $\text{Co}_6\text{W}_6\text{C}$  can survive for relatively long time during the CVD. Finally, we make a simple scheme showing the evolution of Co-W-C catalyst (Figure 5H). The SWCNT is drawn for eye guide only, and it is likely but we do not claim that SWCNTs are formed directly from a certain phase.

However, the findings of this study suggest three possible factors that could contribute to chirality selective growth of SWCNTs. First and most likely, SWCNTs nucleate and precipitate from a certain facet of  $\text{Co}_6\text{W}_6\text{C}$  crystal. As this ternary crystal has a complicated structure, energy matching for a SWCNT on different facets can be different, as has been discussed and predicted in the case of  $\text{Co}_7\text{W}_6$ .<sup>(12)</sup> A second possibility is the role of interface. Along with the loss of W atoms in a  $\text{Co}_6\text{W}_6\text{C}$  particle, oversaturated C can possibly precipitate, particularly at the interface of Co and  $\text{Co}_6\text{W}_6\text{C}$ .<sup>(6, 28)</sup> As steps are clearly observed in the reacted catalyst, how much crystal steps contributed to structure selectivity was argued before but is still not fully concluded. Last, though less likely, the possibility of growth from the pure Co phase cannot be ruled out. Because of the coherent precipitation, certain facets of hcp Co may predominately appear during CVD and promote the formation of (12, 6) SWCNTs. We highlight the second and third mechanisms, i.e. the role of crystal change, on the chirality selective growth particularly after we realize that SWCNT growth is not occurring immediately after the introduction of carbon source. It usually takes more than 30 seconds before we can observe the growth of SWCNTs from SEM, or detect the signal of (12, 6) SWCNTs from Raman. Therefore, it is possible that the nucleation of (12, 6) SWCNT started during the dynamic evolution of our catalyst. Fully clarifying the secrets of chirality-selectivity requires a simultaneous imaging of nanotube and catalyst on  $\text{SiO}_2$  in a statistical manner. Though it is still yet possible in the current study to answer from which sites SWCNTs are formed, this methodology established here has proven its capability of identifying the structure and behavior of complicated catalyst. With clearly illustrated crystal structure and evolution pathways, we believe we have taken a significant step towards unrevealing the mechanism under the chirality selectivity. Also, this method may be applied to other catalysts and high temperature reactions.

## Discussion

We proposed a TEM method which is able to identify the structure, as well as the structure evolution of Co-W-C ternary catalytic nanoparticles during the chirality selective synthesis of SWCNTs. The key was to use a MEMS fabricated  $\text{SiO}_2$  film which is thick enough as the catalyst support but thin enough as observation window. We demonstrated that atomic resolution STEM images can be obtained directly on  $\text{SiO}_2$  film. The Co-W-C ternary catalyst is confirmed to be junctions of W and  $\text{Co}_6\text{W}_6\text{C}$  after

reduction. However, a significant loss of W is observed by quantitative EDS after CVD starts, and finally hcp Co is precipitated coherently from the parent  $\text{Co}_6\text{W}_6\text{C}$  crystal.

One remaining problem in this work is that C is not visible in HAADF images. Though potentially this method is possible to identify a catalyst-SWCNT junction, imaging them simultaneously on  $\text{SiO}_2$  film is still not easy. Therefore, we are unable to conclude from direct imaging at which stage SWCNTs begin to appear, or from which phase direction SWCNTs nucleate. However, as a next step, we might be able to image a SWCNT in TEM mode, and switch to STEM to resolve the atomic structure. Similarly, we noticed the SWCNTs grown by this catalyst is usually curled. It is not impossible that kinks form and change the chirality along one SWCNT. Therefore, being able to grow straight SWCNTs may be crucial for improving chirality enrichment in our samples. Nonetheless, we believe the method proposed here opens up new possibilities for studying nano-sized particles behavior in their original morphologies and in a statistical manner. In particular, the dynamic change before and after a high temperature reactions become possible. More applications, which include but not limited in SWCNT growth, are expected in the future.

## Materials and Methods

### Synthesis of SWCNTs

(12, 6) enriched SWCNTs were grown by alcohol catalytic chemical vapor deposition (ACCVD) method using bimetallic Co-W catalyst prepared by sputtering. Briefly, 0.7 nm W and 0.3 nm Co were sputtered (using UlvacRiko) on the Si/ $\text{SiO}_2$  wafer substrate with an oxide layer of 300 nm. The substrates were then transferred into a tube furnace and heated in Ar/ $\text{H}_2$  (3%  $\text{H}_2$ ) at a pressure of 40 kPa, followed by a reduction at 850°C for 5 min. Then the furnace temperature was reduced to 750°C, and the growth was conducted at 750°C at a low pressure CVD with ethanol as the carbon source (1.3 kPa) for controlled target growth time. After the CVD, ethanol flow was closed and the catalyst was cooled down to the room temperature in the flow of 300 sccm Ar/ $\text{H}_2$  (3%  $\text{H}_2$ ). To study the structure and evolution of catalyst, a similar process was carried out on a Si/ $\text{SiO}_2$  TEM microgrid.

### Characterization of SWCNTs.

The as-grown SWCNT samples were characterized by a scanning electron microscope (SEM, Hitachi S-4800) at an accelerating voltage of 1 kV and a Raman spectrometer (inVia, Renishaw) with the excitation wavelengths of 488, 532, 633, and 785 nm. Raman mapping was performed to obtain more quantitative results about the SWCNT content. Since the spot size of the laser is smaller than 2  $\mu\text{m}$  and the SWCNT length is approximately 2–5  $\mu\text{m}$  as obtained from SEM characterization, an 8  $\mu\text{m}$  spacing is used to avoid the overcounting of the same SWCNT. The equation of  $\omega_{\text{RBM}} = 235.9/d_t + 5.5$  was used to calculate the diameter of SWCNT and  $(n, m)$  assignment was performed according to the method previously proposed. (29)

### TEM/STEM imaging of catalyst.

The low magnification TEM images were obtained by conventional TEMs operated at 200 keV (JEM-2000EX and JEM-2010F, JEOL Co., Ltd). SAED patterns were obtained by a charge-coupled device (CCD) camera or a negative film. A typical camera length is 60 cm and the exposure time is from 2-30 second. Since the diffraction rings of W are very clear, we precisely calibrated the camera-length and it made the other diffraction rings to determine  $\text{Co}_6\text{W}_6\text{C}$  not  $\text{Co}_3\text{W}_3\text{C}$ , which have very similar pattern except

for the lattice parameter. HAADF-STEM, ABF-STEM and EDS were obtained by probe-forming aberration corrected STEM (200 kV, JEM-ARM200F Cold-FEG dual SDD, JEOL Co., Ltd).

### STEM image simulation.

STEM image simulations of  $\text{Co}_6\text{W}_6\text{C}$  were performed by commercially available and accelerated multi-slice simulation software (elbis, BioNet Laboratory Inc.).<sup>(30, 31)</sup> The microscopic parameters in the simulation were set to 200 kV accelerating voltage, an aberration-free probe with a semi-convergence angle of 22 mrad, and a specimen thickness of 6-10 nm.

## H2: Supplementary Materials

### Materials and Methods

Fig. S1 Comparison of SWCNTs grown on Si/SiO<sub>2</sub> substrate and Si/SiO<sub>2</sub> TEM grid.

Fig. S2 Details of the relative surface charge estimation.

Fig. S3 SEM images and Raman spectra of the SWCNTs.

Fig. S4 Low mag. TEM and SAED patterns of Co-W catalyst.

Fig. S5 STEM images of another reacted Co-W-C particle with less W concentration.

## References and Notes

1. S. Iijima, T. Ichihashi, Single-Shell Carbon Nanotubes of 1-Nm Diameter. *Nature* **363**, 603-605 (1993).
2. D. S. Bethune *et al.*, Cobalt-Catalyzed Growth of Carbon Nanotubes with Single-Atomic-Layerwalls. *Nature* **363**, 605-607 (1993).
3. R. Saito, G. Dresselhaus, M. S. Dresselhaus, Physical Properties of Carbon Nanotubes. (1998).
4. R. Saito, M. Fujita, G. Dresselhaus, M. S. Dresselhaus, Electronic-Structure of Chiral Graphene Tubules. *Appl Phys Lett* **60**, 2204-2206 (1992).
5. M. S. Dresselhaus, G. Dresselhaus, R. Saito, C60-Related Tubules. *Solid State Commun* **84**, 201-205 (1992).
6. M. S. He *et al.*, Chiral-Selective Growth of Single-Walled Carbon Nanotubes on Lattice-Mismatched Epitaxial Cobalt Nanoparticles. *Sci Rep* **3**, 1460 (2013).
7. B. L. Liu, F. Q. Wu, H. Gui, M. Zheng, C. W. Zhou, Chirality-Controlled Synthesis and Applications of Single-Wall Carbon Nanotubes. *Acs Nano* **11**, 31-53 (2017).
8. H. Wang *et al.*, Chiral-Selective CoSO<sub>4</sub>/SiO<sub>2</sub> Catalyst for (9,8) Single-Walled Carbon Nanotube Growth. *Acs Nano* **7**, 614-626 (2013).
9. M. M. Shulaker *et al.*, Carbon nanotube computer. *Nature* **501**, 526-530 (2013).
10. C. G. Qiu *et al.*, Scaling carbon nanotube complementary transistors to 5-nm gate lengths. *Science* **355**, 271-276 (2017).
11. A. D. Franklin, ELECTRONICS The road to carbon nanotube transistors. *Nature* **498**, 443-444 (2013).
12. F. Yang *et al.*, Chirality-specific growth of single-walled carbon nanotubes on solid alloy catalysts. *Nature* **510**, 522-524 (2014).
13. H. An *et al.*, Chirality specific and spatially uniform synthesis of single-walled carbon nanotubes from a sputtered Co-W bimetallic catalyst. *Nanoscale* **8**, 14523-14529 (2016).



14. S. C. Zhang *et al.*, Arrays of horizontal carbon nanotubes of controlled chirality grown using designed catalysts. *Nature* **543**, 234-238 (2017).
15. N. Pierce *et al.*, Intrinsic Chirality Origination in Carbon Nanotubes. *Acs Nano* **11**, 9941-9949 (2017).
16. F. Ding, A. R. Harutyunyan, B. I. Yakobson, Dislocation theory of chirality-controlled nanotube growth. *P Natl Acad Sci USA* **106**, 2506-2509 (2009).
17. S. Reich, L. Li, J. Robertson, Control the chirality of carbon nanotubes by epitaxial growth. *Chem Phys Lett* **421**, 469-472 (2006).
18. F. Zhang, P. X. Hou, C. Liu, H. M. Cheng, Epitaxial growth of single-wall carbon nanotubes. *Carbon* **102**, 181-197 (2016).
19. H. Wang *et al.*, Catalysts for chirality selective synthesis of single-walled carbon nanotubes. *Carbon* **81**, 1-19 (2015).
20. D. V. Suetin, I. R. Shein, A. L. Ivanovskii, Structural, electronic and magnetic properties of eta carbides (Fe<sub>3</sub>W<sub>3</sub>C, Fe<sub>6</sub>W<sub>6</sub>C, Co<sub>3</sub>W<sub>3</sub>C and Co<sub>6</sub>W<sub>6</sub>C) from first principles calculations. *Physica B* **404**, 3544-3549 (2009).
21. H. W. Zhu *et al.*, Atomic-resolution imaging of the nucleation points of single-walled carbon nanotubes. *Small* **1**, 1180-1183 (2005).
22. M. H. Hu, Y. Murakami, M. Ogura, S. Maruyama, T. Okubo, Morphology and chemical state of Co-Mo catalysts for growth of single-walled carbon nanotubes vertically aligned on quartz substrates. *J Catal* **225**, 230-239 (2004).
23. D. N. Yuan *et al.*, Horizontally aligned single-walled carbon nanotube on quartz from a large variety of metal catalysts. *Nano Lett* **8**, 2576-2579 (2008).
24. M. Picher, P. A. Lin, J. L. Gomez-Ballesteros, P. B. Balbuena, R. Sharma, Nucleation of Graphene and Its Conversion to Single-Walled Carbon Nanotubes. *Nano Lett* **14**, 6104-6108 (2014).
25. L. L. Zhang *et al.*, Growth Termination and Multiple Nucleation of Single-Wall Carbon Nanotubes Evidenced by in Situ Transmission Electron Microscopy. *Acs Nano* **11**, 4483-4493 (2017).
26. Y. Qian *et al.*, A Comparison Between Reduced and Intentionally Oxidized Metal Catalysts for Growth of Single-Walled Carbon Nanotubes. *Phys Status Solidi B* **255**, 1800187 (2018).
27. A. Markstrom, B. Sundman, K. Frisk, A revised thermodynamic description of the Co-W-C system. *J Phase Equilib Diff* **26**, 152-160 (2005).
28. A. R. Harutyunyan *et al.*, Preferential Growth of Single-Walled Carbon Nanotubes with Metallic Conductivity. *Science* **326**, 116-120 (2009).
29. D. Q. Zhang *et al.*, (n,m) Assignments and quantification for single-walled carbon nanotubes on SiO<sub>2</sub>/Si substrates by resonant Raman spectroscopy. *Nanoscale* **7**, 10719-10727 (2015).
30. F. Hosokawa, T. Shinkawa, Y. Arai, T. Sannomiya, Benchmark test of accelerated multi-slice simulation by GPGPU. *Ultramicroscopy* **158**, 56-64 (2015).
31. F. Hosokawa, H. Sawada, T. Shinkawa, T. Sannomiya, Image transfer with spatial coherence for aberration corrected transmission electron microscopes. *Ultramicroscopy* **167**, 11-20 (2016).

## Acknowledgments

**General:** The authors thank T. Ito and H. Tsunakawa for TEM assistance. H. An thanks the China Scholarship Council for financial support.

**Funding:** Part of this work is financially supported by JSPS KAKENHI Grant Numbers JP25107002, JP15H05760, JP15K17984, and IRENA Project by JST-EC DG RTD, Strategic International Collaborative Research Program, SICORP. Part of this work is based on results obtained from a project commissioned by the New Energy and Industrial Technology Development Organization (NEDO) and by the “Nanotechnology Platform” (project No. 12024046) of the Ministry of Education, Culture, Sports, Science and Technology (MEXT), Japan.

**Author contributions:** S.M. and R.X. designed the experiment. H.A. performed the catalyst preparation, SWCNT growth and chirality characterization. R.X. estimated the charge distribution. H.A. and R.X. took the SAED patterns, A.K. and R.X. carried out the TEM/STEM imaging. H.A. C.B. and A.L. performed the structure analysis. A.K. simulated the STEM images and performed the EDS mapping. R.X., A.K., H.A. wrote the paper. All authors joined the discussion and interpretation of the results.

**Competing interests:** The authors declare no competing interests.

**Data and materials availability:** All data needed to evaluate the conclusions in the paper are present in the paper and/or the Supplementary Materials. Additional data related to this paper may be requested from the authors.

## Figures and Tables

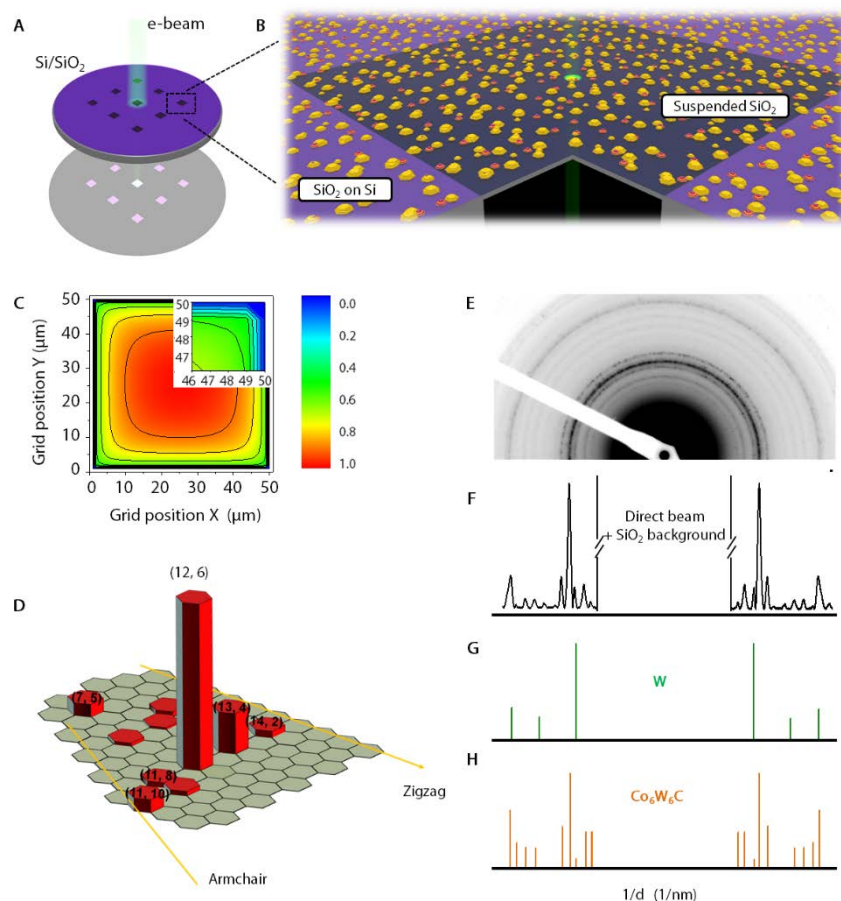


**Figure 1 Overview of the proposed TEM method, produced SWCNTs, and the structure of catalyst.** (A) A schematic of the 3 mm diameter Si/SiO<sub>2</sub> TEM grid. (B) The enlarged schematic showing a 20 nm thin suspended SiO<sub>2</sub> serves as the TEM observation window, and catalyst can be prepared directly on this film and dispersed uniformly. (C) An estimated distribution of charge density over the suspended SiO<sub>2</sub> film, suggesting that electron accumulation at edges and corners of the window is less than 10% of the value in the center. (D) Chirality distribution of SWCNTs synthesized from Co-W-C catalyst. (E) A typical SAED pattern of reduced Co-W-C catalyst. (F) Intensity profile of SAED pattern in (E). (G) (H) standard pdf card of metallic W (#04-0806) and Co<sub>6</sub>W<sub>6</sub>C (#23-0939).

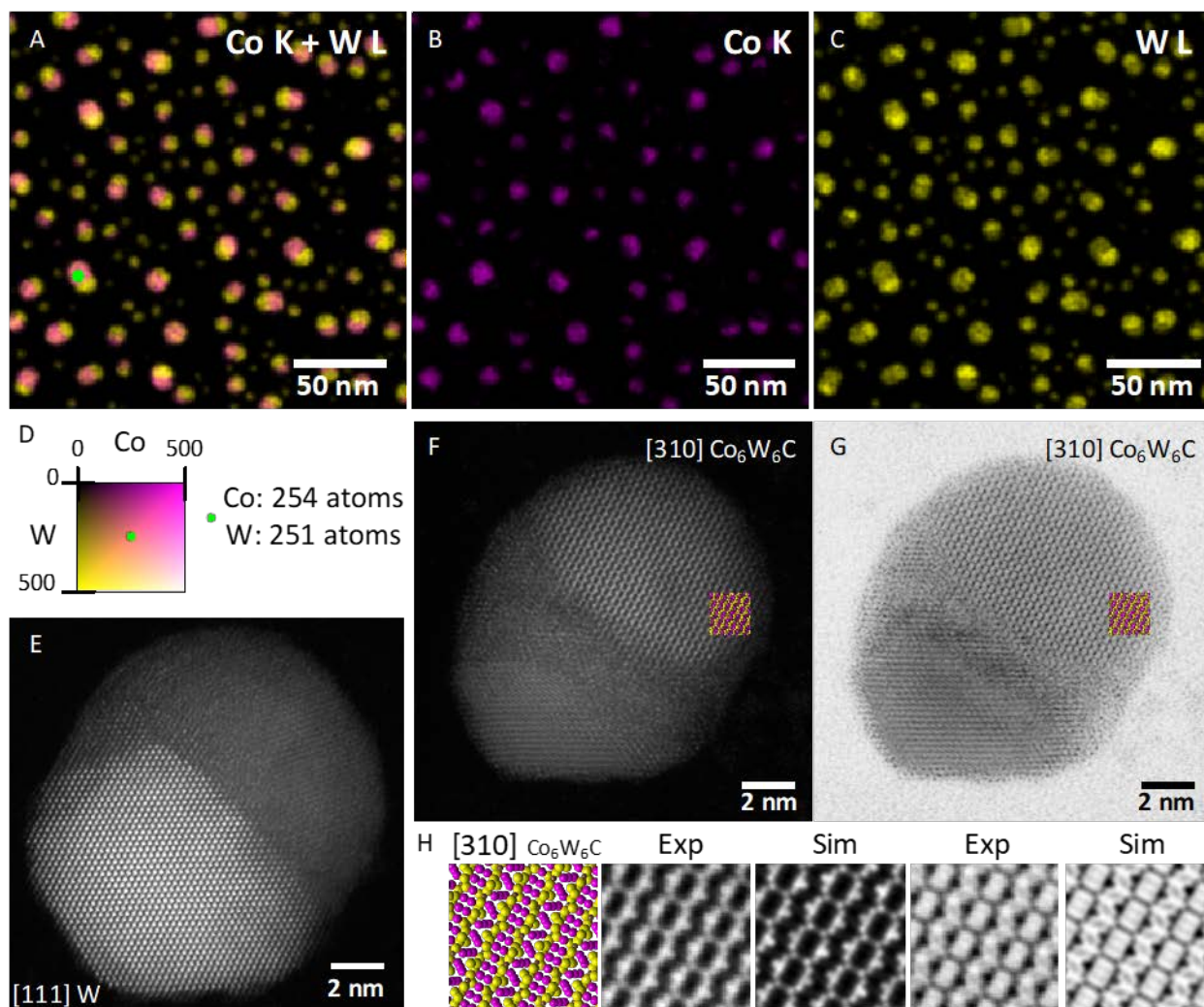


**Figure 2 Atomic structure identification of Co-W-C.** (A-D) Quantitative EDS mapping of reduced Co-W-C catalyst on suspended  $\text{SiO}_2$  film, suggesting two types of particles are existing: I. pure W and II. Junctions of pure W and Co-W mixtures. (E) HAADF image of a junction particle viewed from the [1 1 1] direction of the bottom part, suggesting it is a metallic bcc-W phase. (F) Dark field and (G) Bright field STEM image of the same particle tilted to the [3 1 0] axis of the upper half of the particle, suggesting a  $\text{Co}_6\text{W}_6\text{C}$  phase. (H) The structure model and comparison of experimental and simulated bright and dark field STEM images of  $\text{Co}_6\text{W}_6\text{C}$  from the direction of [310].

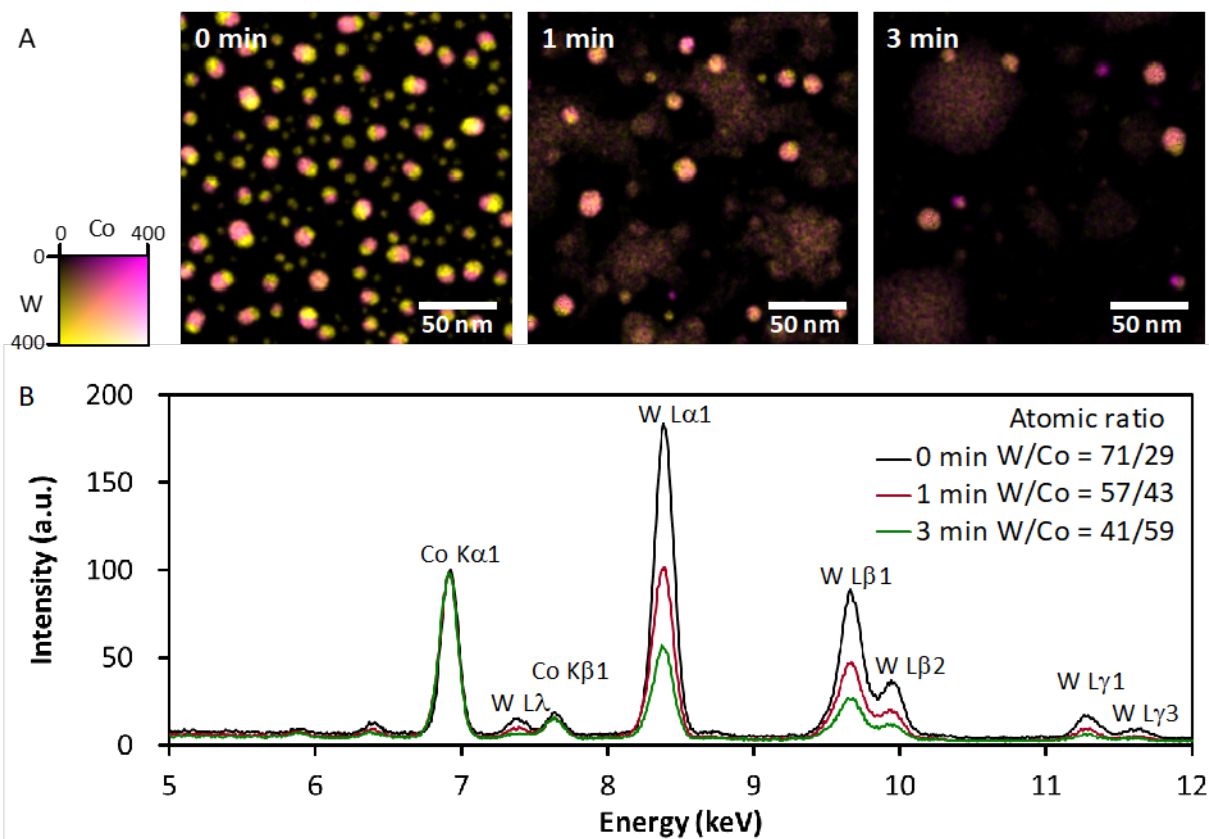


**Figure 3 Elemental evolution of Co-W-C after different CVD time.** (A) Quantitative EDS mappings of reduced and reacted Co-W-C catalyst particles on Si/SiO<sub>2</sub> grids. (B) Typical EDS spectra of different samples, showing a clear decrease of atomic ratio of W:Co along with CVD.

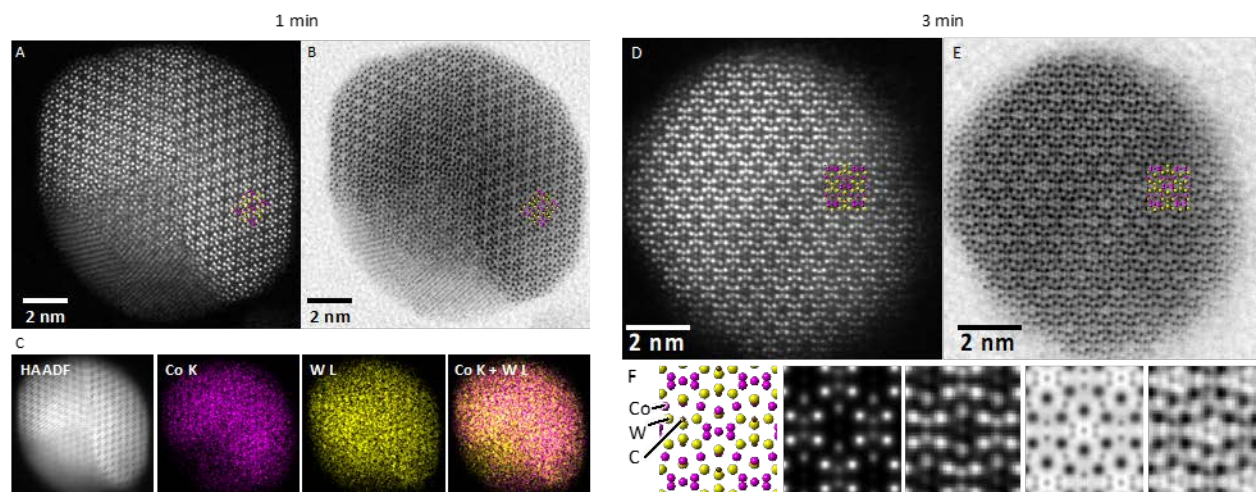


**Figure 4 Structure evolution of Co-W-C during CVD.** (A) DF and (B) BF STEM images and (C) EDS mapping of reacted Co-W-C catalyst after a 1 min CVD, showing the particle is a junction of W-enrich phase and  $\text{Co}_6\text{W}_6\text{C}$  but W enriched phase are much smaller than those pure W in the reduced catalyst. (D) DF and (E) BF STEM images and (F) structure model, comparison of simulated and experimental STEM images of reacted Co-W-C catalyst after a 3 min CVD, showing this particle contains only  $\text{Co}_6\text{W}_6\text{C}$  phase and W enriched phases disappeared after a 3 min CVD.



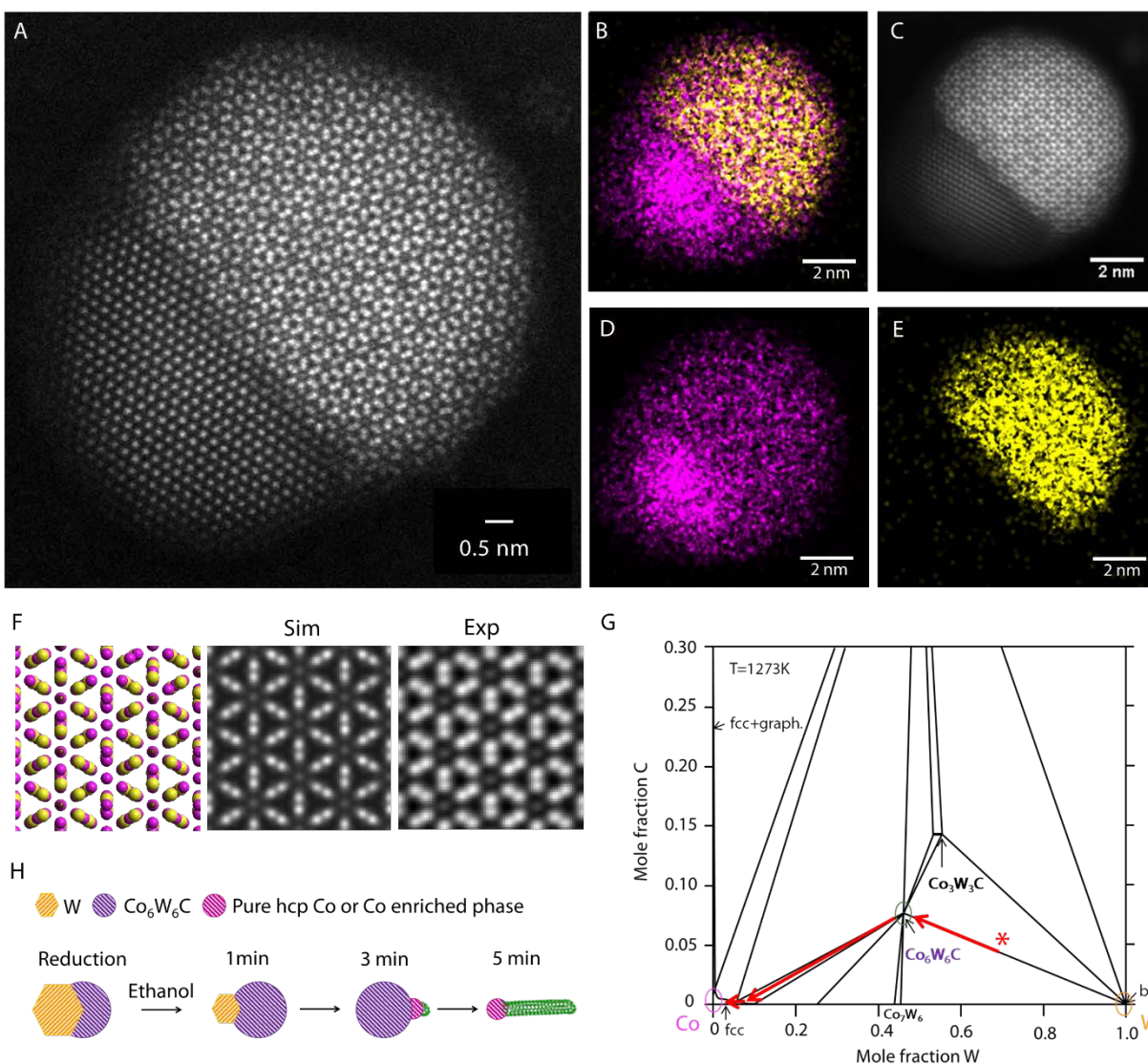


**Figure 5 Precipitation of Co and Co-enriched phase.** (A) An atomic resolution HAADF-STEM image of a 3 min reacted Co-W-C catalyst particle, showing the particle is a junction of  $\text{Co}_6\text{W}_6\text{C}$  and pure Co phase. (B)-(E) EDS mapping of the same particle (pink represents Co K and yellow represents W L) and HAADF-STEM image taken simultaneously during EDS mapping; (F) a comparison between simulated and experimental STEM image of  $\text{Co}_6\text{W}_6\text{C}$ . These results suggest an oversaturation and precipitation of Co or Co-enriched phase from  $\text{Co}_6\text{W}_6\text{C}$  when the CVD time is extended. (G) A bulk phase diagram of Co-W-C ternary system remade from ref. 27. (H) A schematic showing the overall process revealed in this work, and a possible nucleation mechanism of SWCNTs. (pink and yellow)

FRONT MATTER

**Atomic Scale Structural Identification and Evolution of Co-W-C Ternary SWCNT Catalytic Nanoparticles: HR-STEM imaging on SiO<sub>2</sub>**

Hua An,<sup>1†</sup> Akihito Kumamoto,<sup>2†</sup> Rong Xiang,<sup>1†\*</sup> Taiki Inoue,<sup>1</sup> Keigo Otsuka,<sup>1</sup> Shohei Chiashi,<sup>1</sup> Christophe Bichara,<sup>3</sup> Annick Loiseau,<sup>4</sup> Yan Li,<sup>1,5</sup> Yuichi Ikuhara<sup>2</sup>, Shigeo Maruyama<sup>1,6\*</sup>

<sup>1</sup>Department of Mechanical Engineering, The University of Tokyo, Tokyo 113-8656, Japan

<sup>2</sup>Institute of Engineering Innovation, The University of Tokyo, Tokyo 113-8656, Japan

<sup>3</sup>CINAM, CNRS and Aix Marseille Université, Campus de Luminy, Case 913, 13288 Marseille Cedex 9, France

<sup>4</sup>Laboratoire d'étude des microstructures, CNRS-ONERA, 92322 Châtillon, France

<sup>5</sup>College of Chemistry and Molecular Engineering, Peking University, Beijing 100871, China

<sup>6</sup>Energy NanoEngineering Laboratory, National Institute of Advanced Industrial Science and Technology (AIST), Tsukuba 305-8564, Japan

†These authors contributed equally to this work.

\*Corresponding author. Email: xiangrong@photon.t.u-tokyo.ac.jp (R.X.); maruyama@photon.t.u-tokyo.ac.jp (S.M.)



## Supplementary Materials

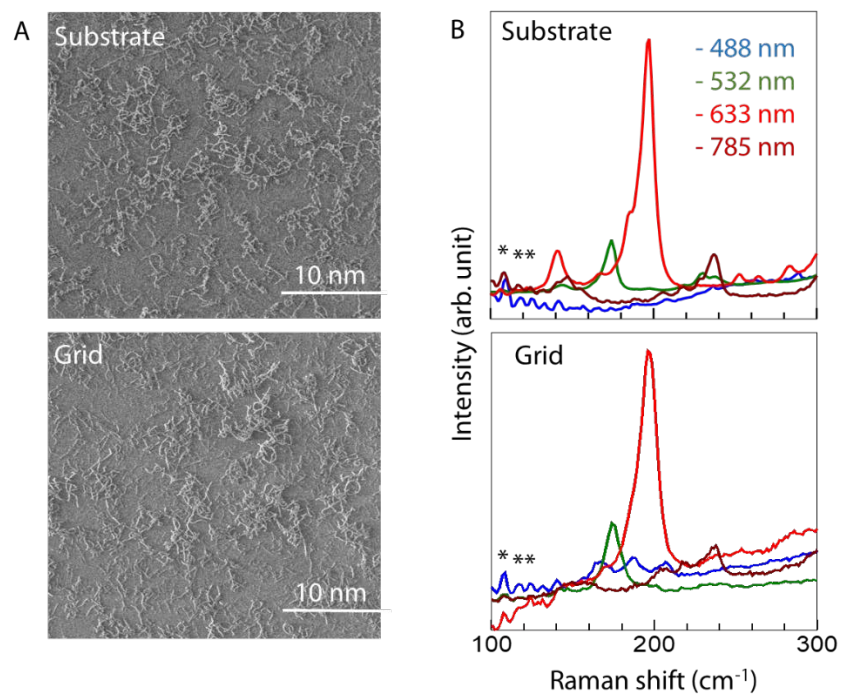
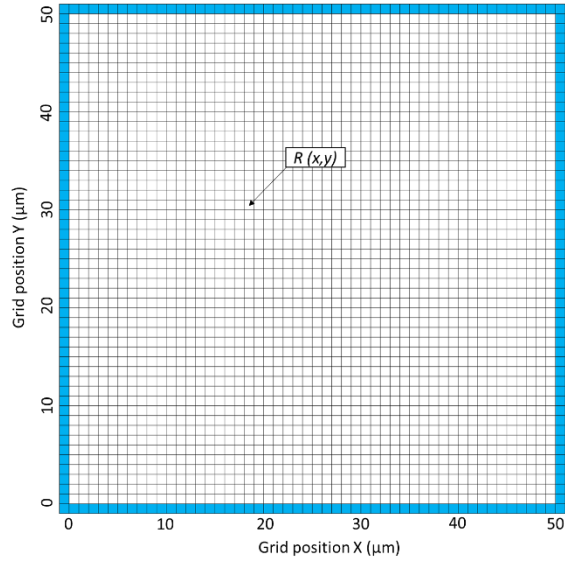


**Fig. S1 Comparison of SWCNTs grown on Si/SiO<sub>2</sub> substrate and the Si/SiO<sub>2</sub> TEM grid.** (A) SEM images and (B) averaged Raman spectra of obtained SWCNTs on normal substrate and the TEM grid, showing a similar morphology and chirality distribution. Asterisks suggest the artifact peaks from the measurement.



- SiO<sub>2</sub> on silicon
- suspended SiO<sub>2</sub>

Assumption:

1. The suspended SiO<sub>2</sub> film is divided into 50 × 50 pitches, described as (x,y);
2. Each pitch (1 μm × 1 μm) has the same, constant resistance;
3. The pitch next to an edge (x=1 OR y=1 OR x=50 OR y=50), resistance to Si is zero.

If  $x \neq 1$  AND  $y \neq 1$  AND  $x \neq 50$  AND  $y \neq 50$

$$R(x,y) = \left( \sum_{i=1}^{50} (abs(x-i) + abs(y-1))^{-1} \quad //parallel\ resistance\ to\ lower\ Si \right.$$

$$+ \sum_{j=1}^{50} (abs(x-1) + abs(y-j))^{-1} \quad //parallel\ resistance\ to\ left\ Si$$

$$+ \sum_{l=1}^{50} (abs(x-i) + abs(y-50))^{-1} \quad //parallel\ resistance\ to\ top\ Si$$

$$\left. + \sum_{j=1}^{50} (abs(x-50) + abs(y-j))^{-1} \right)^{-1} \quad //parallel\ resistance\ to\ right\ Si$$

If  $x=1$  OR  $y=1$  OR  $x=50$  OR  $y=50$

$$R(x,y) = 0$$

**Fig. S2 Details of the relative surface charge estimation.** The relative surface charge density is estimated under the following simplification and assumptions. 1) the suspended SiO<sub>2</sub> film is divided into 50 × 50 pitches, which have the same resistance; 2) the Si under SiO<sub>2</sub> is considered as the good conductor and ground state (potential zero, blue pitches in the figure); 3) the surface charge of each pitch at constant current (certain beam density in TEM) is proportional to its resistance to potential zero position, 4) the total resistance at each pitch,  $R(x, y)$ , is the parallel resistance to all Si pitches (lower, left, top and right); 5) the pitch next to a Si has a zero resistance to Si.

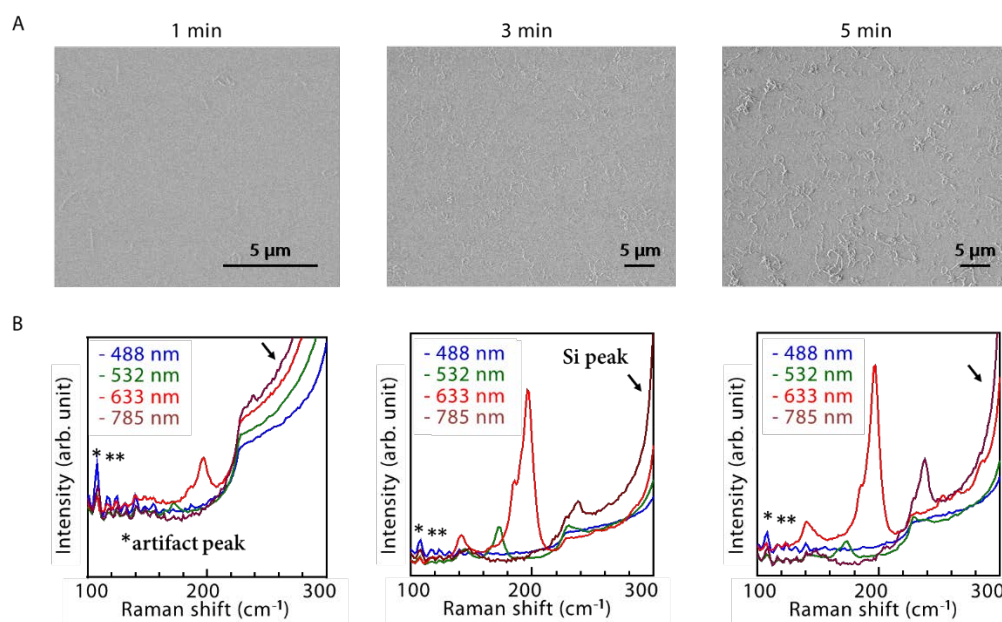


**Fig. S3 SEM images and Raman spectra of the SWCNTs.** (A) Representative SEM images of SWCNT samples after different growth time, showing most SWCNTs grown at ~ 3 min. (B) Raman spectra of SWCNTs with the same growth time, suggesting the best selectivity is at a CVD time of ~ 3 min, and after 5 min, growth selectivity decreases.

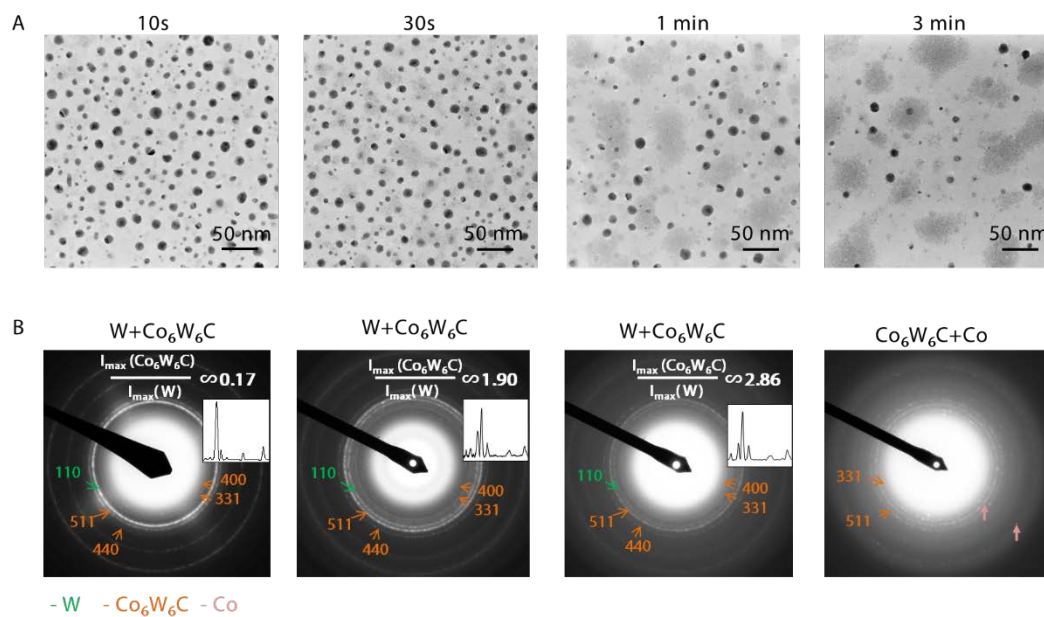


**Fig. S4 Low mag. TEM and SAED patterns of Co-W catalyst.** (A) Morphology of Co-W catalyst dependent on growth time. (B) Electron diffraction pattern at different growth time showing the catalyst structure, and the comparison of the relative intensity ratio of  $\text{Co}_6\text{W}_6\text{C}$  and W according to the intensity profile in the insets.

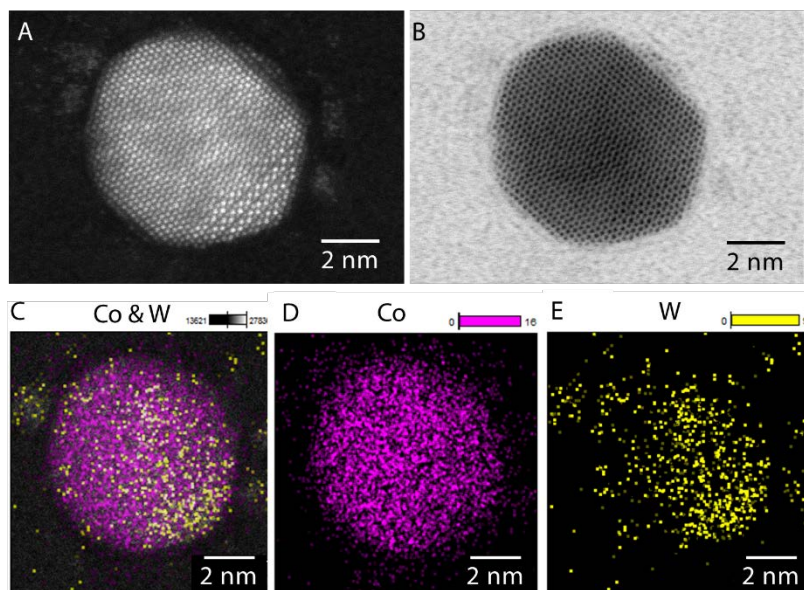


**Fig. S5 STEM images of another reacted Co-W-C particle with less W concentration.** (A)-(B) STEM images and (C)-(E) EDS mapping of another particle in the 3 min reacted Co-W-C catalyst. The structure is similar to the particle shown in the main text but the Co-enriched area is larger.